Ordering of Cylindrical Domains of Block Copolymers under Moving Temperature Gradient: Separation of ∇T-Induced Ordering from Surface-Induced Ordering

Kazuki Mita,[†,||] Hirokazu Tanaka,[†,||] Kenji Saijo,[†] Mikihito Takenaka,[†,‡] and Takeji Hashimoto*[,†,§]

Department of Polymer Chemistry, Graduate School of Engineering, Kyoto University, Katsura, Nishikyo-ku, Kyoto 615-8510, Japan; Structural Materials Science Laboratory, SPring-8 Center, RIKEN Harima Institute Research, Hyogo 679-5148, Japan; and Advanced Science Reserch Center (ASRC), Japan Atomic Energy Agency (JAEA), Tokai-mura, Ibaraki-Pref. 319-1195, Japan

Received February 19, 2008; Revised Manuscript Received May 19, 2008

ABSTRACT: In a previous paper [Mita et al. *Macromolecules* **2007**, *40*, 5923], we reported that the zone heating method applied to the block copolymer bulk forming hexagonally packed cylindrical (hex-cyl) microdomain structure enables to develop unique columnar grains macroscopically extended along the temperature gradient (∇T) axis and that within the grain hex-cyl has a fixed orientation: Both the cylinder axis and the (100) plane of hex-cyl are normal to the ∇T axis, and the rotational angle of the cylinder around the ∇T axis is fixed also. We believe the method involves the ordering under two external fields coupled together: one is a field induced by a glass surface, and the other is a field induced by a moving ∇T. In this paper, we aim to separate effects of the two fields on the ordering of hex-cyl in order to clarify the effects intrinsic in the moving ∇T field. For this purpose, we tilt the glass surface with respect to ∇T direction by an angle of 45°. Small-angle X-ray scattering studies revealed that the moving ∇T itself can create the columnar grain texture, independent from the surface-induced ordering effect: The effects of the moving ∇T field become dominant over those of the glass-surface field with an increase of the distance from the glass surface.

1. Introduction

We reported oriented columnar grains having macroscopic orientation of hexagonally packed cylindrical microdomain structure (hex-cyl) developed under the zone heating method.[1] With this method, we imposed a moving temperature gradient (∇T), during the ordering process from the disorder state, on polystyrene-*block*-polyisoprene (SI) diblock copolymer (dibcp) which forms hex-cyl composed of polystyrene (PS) block chains in the matrix of polyisoprene (PI) block chains in the absence of external fields. The special texture of hex-cyl induced by the zone heating method has following features: (1) The texture developed consists of volume-filled columnar grains with the grain axis extended parallel to the ∇T axis (defined as Oz axis). (2) Within the grains the cylinder axis and the (100) plane of hex-cyl orient perpendicular to the ∇T axis. (3) Although the cylinder axis has a rotational freedom around the ∇T axis, the rotational angle is expected to be fixed within a given grain but to vary among different grains.

We proposed that the intriguing texture thus obtained is a consequence of the two external fields coupled together and enhancing each other: (i) the field given by interactions between the glass surface and polymers and (ii) the field given by the ∇T field. The field (i) gives rise to the surface-directed ordering[2−7] near the order−disorder transition (ODT) temperature (T_{ODT}) with a uniaxial symmetry around the unit normal vector of the glass surface $\mathbf{n}_g$. The field (ii) gives rise to a continuous growth of the grains developed by the field (i) with a uniaxial symmetry around the ∇T axis. In the previous work, we set both the ∇T axis and $\mathbf{n}_g$ parallel, and hence the two external fields are expected to work cooperatively in the ordering process of the hex-cyl microdomains via ODT, giving rise to the intriguing texture with a special orientation of hex-cyl as summarized above in items (1)−(3).

In this work we aim to explore the effects of the ∇T field separately from the effects of the glass-surface field. For this purpose we tilted $\mathbf{n}_g$ with respect to ∇T by 45° in the zone heating process as shown in Figure 1, so that the surface-induced ordering tends to align hex-cyl with respect to $\mathbf{n}_g$, while ∇T-induced ordering tends to align hex-cyl with respect to the ∇T axis (z axis). More specifically or precisely, the glass-surface induced ordering is expected to grow the columnar grains with their long axes and the reciprocal lattice vector of the (100) plane of hex-cyl within the grains oriented parallel to $\mathbf{n}_g$. This direction is different from that of the ∇T axis by 45°. We focus on how this mismatch in the directions of the two fields affects the texture and orientation of the hex-cyl. Consequently, a relative contribution of the two external field is anticipated to vary with a distance z from the inclined glass surface, which would provide insights for the separation of the two effects.

This idea for the separation of the two effects was originally introduced by Hashimoto et al.[8] for the zone-heating method

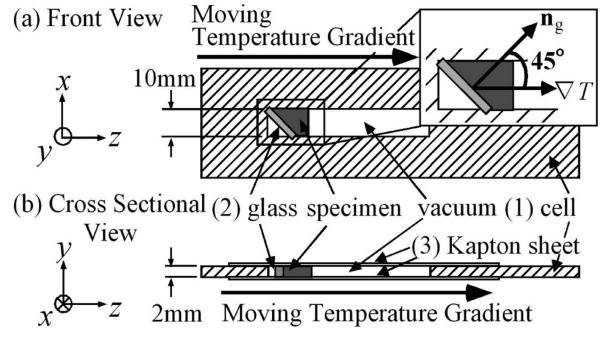

Figure 1. Schematic illustration of the sample cell used for the zone heating device: (a) top view and (b) cross-sectional view through the center line of (a). The film specimen was placed inside the cell made out of poly(tetrafluoroethylene) (PTFE) [part (1)] with a glass surface [part (2)]. The normal vector of the glass surface ($\mathbf{n}_g$) was set at an angle of 45° with respect to the ∇T axis. Thin polyimide sheets (Kapton) [part (3)] were placed on both sides of the PTFE cell normal to Oy axis.

* To whom correspondence should be addressed.
† Kyoto University.
‡ RIKEN Harima Institute Research.
§ Japan Atomic Energy Agency.
|| Present address: R&D Center, Mitsui Chemicals, Inc., 580-32 Nagaura, Sodegaura, Chiba 299-0265, Japan.

10.1021/ma800361d CCC: $40.75
Published on Web 08/22/2008

Table 1. Characteristics of the Samples Used in This Work[a]

code	M_n	M_w/M_n	f_{PS}	T_{ODT} (°C)
SI-1	3.1×10^4	1.01	0.33	191
HI	1.2×10^3	1.08	0	
SI-1/HI(95/5)			0.31	178

[a] M_n = number-average molecular weight estimated by gel permeation chromatography (GPC); M_w/M_n = polydispersity index where M_w is weight-average molecular weight measured by GPC; f_{PS} = volume fraction of polystyrene estimated by using M_n of each block in SI-1 and that of HI and assuming densities of PS and PI in the system to be equal to those of corresponding homopolymers;[20,21] T_{ODT} = order−disorder transition temperature evaluated by SAXS.

applied to a lamella-forming SI dibcp. They qualitatively indicated a crossover from the dominance of the glass-surface-induced ordering to the dominance of the ∇T-induced ordering with increasing z from the glass surface: critical distance for the crossover was found to be less than 1 mm from the glass surface. In this work we shall explore whether the crossover occurs for a hex-cyl forming block copolymer. It is important to note here a difference of the two systems; lamella and hex-cyl order respectively into one- and two-dimensionally periodic structure. Whether or not the crossover occurs for hex-cyl and, if it occurred, how the crossover is affected by the dimensionality of the ordered structure are not known yet at all. Therefore, the exploration of the crossover is believed to be important not only in physical science of bcps but also in that of soft matters in general. Moreover, if the crossover exists, we aimed to explore it in much more quantitatively than the previous work,[8] as the previous work was too qualitative, and to present a possible model, as the previous work did not mention it at all.

The same zone heating apparatus and sample cell as those used in the previous work[1,9] were used in this work. We set the same Cartesian coordinate as that in the previous work[1] where Oz axis is parallel to the ∇T axis. We set a positive ∇T between T_1 and T_2 across T_{ODT} such that $T_1 < T_{ODT} < T_2$. The ∇T zone moved continuously from the left edge to the right edge of the sample along Oz axis, giving rise to a sequential ordering of the sample from a disordered to an ordered state from the glass surface side of the sample toward its interior. For the detailed method of zone heating and the principle concerning the directed ordering process readers should refer to the previous work.[1]

We would like to note that there are also a number papers on the zone annealing of bcps. They are computational[10,11] and experimental studies[12,13] on two-dimensional systems and thin films, respectively. We shall discuss our results in the light of those reported results later in section 4.4.

2. Experimental Method

2.1. Sample. The samples used in this study were the same SI dibcp (SI-1) and homopolyisoprene (HI) as previously used,[1] and the characteristics of polymers are summarized in Table 1. We used the same blended sample of SI-1 and HI with the same blending ratio of SI-1/HI = 95/5 wt % as previously used. The sample preparation method was detailed previously so that we shall not repeat to describe it here. The SAXS study of the sample designated SI-1/HI(95/5) revealed that the Bragg spacing for the (100) plane, D_{100}, was 22 nm, and T_{ODT} was at 178 °C. The reason for blending HI and SI is to enhance the (110) diffraction intensity from hex-cyl as detailed elsewhere.[1]

2.2. Zone Heating. Figure 1 shows the specimen cell used in the zone heating device. The film specimen of 2 mm thickness and 10 mm width was placed inside the cell made of poly(tetrafluoroethylene) (PTFE) [part (1)]. Temperature gradient ∇T and its moving direction were set along the Oz direction. We attached a piece of glass [part (2)] to the cell with an angle of 45° between $\mathbf{n}_g$ and the Oz axis. The specimen was in contact with thin polyimide (Kapton) sheets [part (3)] on both sides of specimen surfaces parallel

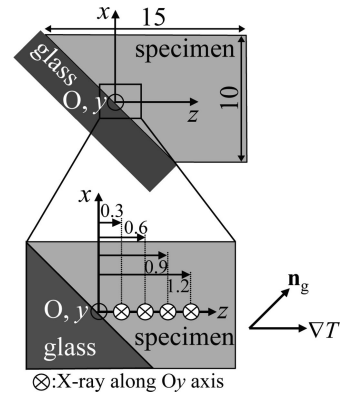

Figure 2. Schematic diagram indicating geometric relationships among incident X-ray beam, the specimen, and the Cartesian coordinate. The origin of the Cartesian coordinate was set at the center of the glass surface which contacts with the specimen surface. The numbers are expressed in unit of "mm". In order to clarify the positional dependence of the orientation of hex-cyl along the z direction, the incident beam irradiated parallel to the Oy axis was shifted along the Oz axis, keeping $x = 0$ and $y = 0$.

to the Oxz plane.[14] In this experiment, we applied a sharp nominal temperature gradient of $|\nabla T|_{nom}$ = 73 °C/mm between the high temperature T_2 = 225 °C and the low temperature T_1 = 5 °C across T_{ODT} = 178 °C. The moving rate of ∇T was 75 nm/s (3.4D_{100}/s), which was the slowest velocity in the range where we can apply to our specimens without the thermal degradation of the specimen. The effective temperature gradient $|\nabla T|_{eff}$ actually set to the specimen and measured was 42 °C/mm (9.2×10^{-4} °C/D_{100}), much smaller than $|\nabla T|_{nom}$, which may be due to conduction of heat within the specimen.[1] These conditions are the same as those previously used,[1] except for the tilting of the glass surface.

It is important to note that the Kapton sheets which confine the 2 mm thick specimens does not affect at all the specific orientation and texture of hex-cyl created by the zone heating method through the glass-surface-induced ordering, as clarified in ref 1. The sheets used are stable thermally at 225 °C.

2.3. Small-Angle X-ray Scattering (SAXS). SAXS measurements with the in-house SAXS apparatus were conducted at room temperature for the specimen subjected to the zone heating process. The in-house SAXS apparatus used in this experiment consists of a 18 kW rotating-anode X-ray generator (M18X HF by Bruker Co. Ltd., Japan) operated at 14 kW, a graphite crystal for incident beam monochromatization, a 2116 mm camera (705 mm from the source to the sample and 1411 mm from the sample to the detector) including two pinholes having diameter 0.3 mm between the source and the sample, and a 2D imaging plate (IP) detector.[15] The Cu Kα line (λ = 0.154 nm) was used as an incident beam. The beam at the sample surface had a circular shape with the radius of 0.3 mm.

We set the Cartesian coordinate Oxyz fixed to the specimen with its origin right in the middle of the glass surface which contacts with the specimen surface, as shown in Figure 2. In order to investigate a positional dependence of the ordered hex-cyl with respect to z, the incident beam position was changed along the Oz direction, e.g., z/mm = 0.3, 0.6, 0.9, and 1.2 (Figure 2), keeping $x = 0$ and $y = 0$ and keeping the incident beam irradiated along the Oy direction. Exposure time for taking a 2D SAXS pattern at each z position was 900 s.

3. Results

2D SAXS patterns obtained for z/mm = 0.3, 0.6, 0.9, and 1.2 are shown in parts a, b, c, and d of Figure 3, respectively. q_x and q_z are x and z components of the scattering vector $\mathbf{q}$. The patterns (e) and (f) will be discussed later in section 4.2. The pattern varies with z. At z = 0.3 mm (Figure 3a), the diffraction from the (100) plane of hex-cyl gives a two-point pattern or two-arc pattern with its maximum intensity along the $\mathbf{n}_g$ direction. On the other hand, at z = 1.2 mm (Figure 3d), the diffraction from

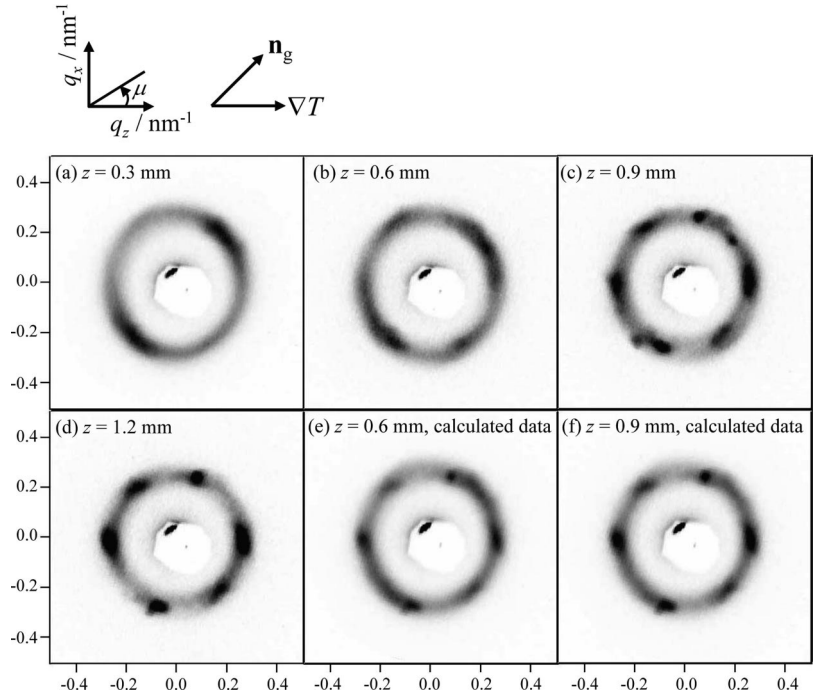

Figure 3. 2D-SAXS patterns obtained by irradiating incident X-ray beams parallel to Oy direction at a fixed position of $x = 0$ and $y = 0$ but by changing the incident beam position along the temperature gradient direction (Oz direction): z/mm = 0.3 (a), 0.6 (b), 0.9 (c), and 1.2 (d). Parts (e) and (f) are the calculated patterns at z/mm = 0.6 and 0.9, respectively (see section 4.2).

the (100) plane gives the six-point pattern with the two points along the Oz direction having an enhanced intensity. This six-point pattern has the essentially same characteristic as that for the hex-cyl obtained by the zone heating with the nontilted glass surface, as reported in our previous paper.[1] The 2D SAXS patterns obtained at z/mm = 0.6 and 0.9 exhibit characteristics intermediate between those at z/mm = 0.3 and 1.2, as will be discussed later in section 4.2. These results seem to infer that the field which dominantly controls the orientation of hex-cyl changes from the glass-surface field to the moving-∇T field with increasing z, as will be detailed later in section 4.3.

The z-dependence of the SAXS patterns as described above appears to be superficially similar to those previously reported on that for the lamella-forming bcp.[8] The two-point patterns or two-arc patterns in the previous report reflect orientation of the lamellar normals $\mathbf{n}_l$, while the SAXS patterns in this work reflect orientation of (100) plane of hex-cyl. Depending on degree of the orientation of hex-cyl, the SAXS patterns show not only the two-arc pattern but also the six-point pattern, as shown in Figure 3. Thus, the information obtained from the SAXS patterns in the previous report and that in the present work are different, which reflects the difference of the system having a one-dimensional order and that having a two-dimensional order.

4. Discussion

4.1. Glass-Surface Induced Ordering and ∇T-Induced Ordering. In order to quantitatively analyze the change in the ordered texture and orientation of hex-cyl with z from the SAXS patterns shown in Figure 3a−d, the μ dependence of the (100) diffraction intensity in each SAXS pattern was measured and compared in Figure 4, where the measured profiles are shown by open circles. The solid line drawn for the profiles at z/mm = 0.6 and 0.9 will be discussed later in section 4.2. The profiles at z/mm = 0.3 exhibit peaks at $\mu = 45°$ and 225° along the direction parallel to $\mathbf{n}_g$. This profile implies the glass-surface-induced orientation of hex-cyl with the (100) plane preferentially oriented perpendicular to $\mathbf{n}_g$, as will be discussed below in conjunction with Figure 5a.

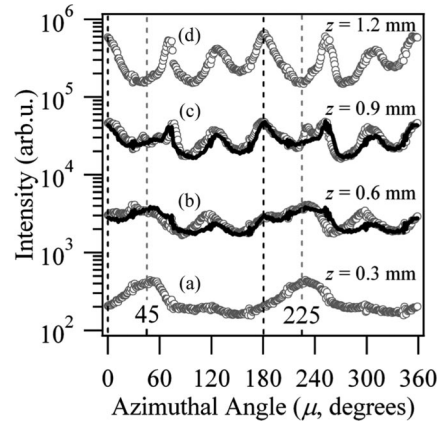

Figure 4. μ dependence of the (100) diffraction intensity in each SAXS pattern shown in Figure 3a−d (circular symbol). The intensities of the data at z/mm = 0.3 are actual values, and those of other data were shifted up vertically by 1 decade relative to the intensities immediately below. The solid lines in parts (b) and (c) are the calculated μ dependence of the (100) diffraction intensity at z/mm = 0.6 and 0.9.

Figure 5a shows the schematic illustration of the orientation induced by the glass surface.[1] The cylinder axis is perpendicular to $\mathbf{n}_g$, but the rotation of the axis around $\mathbf{n}_g$ (defined by the angle γ in Figure 5c) is uniform so that the axis is confined parallel to the glass surface but is random in the plane parallel to the glass surface. The diffraction from the (100) plane for the hex-cyl having orientation as specified in Figure 5a should give the six-point 2D SAXS pattern observed in the q_xq_z plane in which the two points at $\mu = 45°$ and 225° have an enhanced intensity and the four points at $\mu = 105°$, 165°, 285°, and 345° have a weak but equal intensity, as elucidated previously.[1] However, the experimental pattern shown in Figure 3a or the μ dependence of the profile shown in Figure 4a exhibits only the two peaks at $\mu = 45°$ and 225°, which are superposed by an essentially circular diffraction ring where the intensity is independent of μ. Though we show a perfectly oriented model in Figure 5a, the circular ring or the broadening of the diffraction

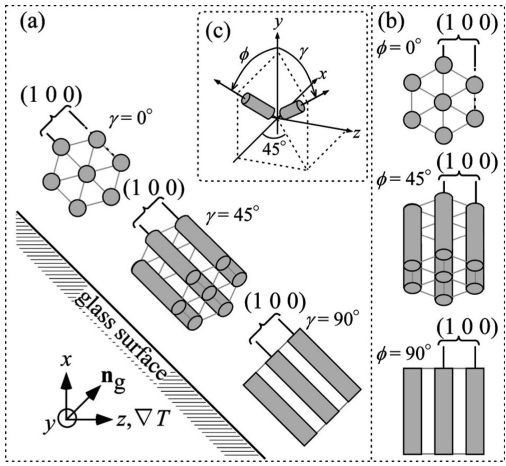

Figure 5. Models for (a) glass-surface-induced ordering and (b) moving-∇T-induced ordering of hex-cyl. In the glass-surface-induced ordering, the (100) planes are perpendicular to the normal vector of glass surface ($\mathbf{n}_g$), while in the moving-∇T-induced ordering, the (100) planes are perpendicular to the ∇T axis (z axis). ϕ and γ defined in (c) are the rotational angle of cylinder axis around z axis and around $\mathbf{n}_g$ axis, respectively.

intensity along μ indicates that there exist (i) a distribution of the rotational angle around cylinder axis and (ii) a distribution of the angle between the reciprocal vector of (100) plane ($\mathbf{n}_{100}$) and $\mathbf{n}_g$ in the real system at z/mm = 0.3. This circular ring is considered to bury the four-point pattern having the intensity maxima at μ = 105°, 165°, 285°, and 345°. The two-point pattern having the intensity maxima at μ = 45° and 225° are enhanced, simply because all the orientations of the hex-cyl in Figure 5a from γ = 0° to 180° contribute to the two points, while the other four points arise only from the orientation of γ = 0°. The existence of the contribution of the circular diffraction ring at z/mm = 0.3 may be explained by the relationship between the growth rate of the grains having glass-surface-induced ordering along ∇T direction and the moving rate R, as will be discussed later in section 4.3.

As shown in Figure 4, intensities at μ = 45° and 225° decrease with z and completely decay in the data obtained at z/mm = 1.2. This result indicates that the dominance of the glass-surface-induced orientation of hex-cyl decays with increasing z and that there will be no glass-surface-induced ordering effects in the position of z/mm = 1.2. Instead of the peaks at μ = 45° and 225°, the peaks at μ = 0°, 60°, 120°, 180°, 240°, and 300° appear and their intensities increase with z. At z/mm = 1.2, the μ dependence of the (100) diffraction intensity has the same characteristics as that found for the zone-heated specimen with the nontilted glass surface.[1] This result indicates that the moving-∇T field itself can induce the characteristic ordering with the specific orientation of hex-cyl as schematically illustrated in Figure 5b, free from the effect of the glass surface. In the model of Figure 5b, the (100) planes are perpendicular to the ∇T axis. The cylinder axis is confined parallel to xy plane but is randomly oriented around ∇T axis (Oz axis). The rotational angle ϕ of cylinder axis around the ∇T axis is uniform from 0° to 180°.

The increase of the dominance of ∇T-induced orientation with z was also observed in another experiment where the bcp, which forms hex-cyl of PI in the matrix of PS, was zone-heated at R = 25 nm/s with the tilted glass surface in the same way as in this paper.

4.2. Positional Dependence of Orientation of Hex-Cyl along the ∇T Direction. As a first step to analyze how the influences of the surface-induced ordering and those of the moving ∇T-induced ordering change with z, we assume that the μ dependence of (100) diffraction intensity as a function of z, $I(\mu;z)$, can be described by the linear combination of the μ dependence of diffraction intensity at z/mm = 0.3 and 1.2

$$I(\mu;z) = w_{0.3}(z)\, I_{0.3}(\mu) + w_{1.2}(z)\, I_{1.2}(\mu), \quad w_{0.3}(z) + w_{1.2}(z) = 1 \tag{1}$$

with the weight fraction of the respective diffraction intensity varying with z. This assumption should be valid if the hex-cyl grains created with the zone heating under the tilted glass condition are a mixture of the following two types of grains: grains created through the tilted glass-surface-induced ordering and grains created through the ∇T-induced ordering. Moreover, we assume that the former grains give the μ dependence at z = 0.3 mm, while the latter grains give the μ dependence at z = 1.2 mm and that the weight fraction of each grain vary with z.

On the basis of the above assumption, we tried to fit the μ dependence of (100) diffraction intensity at z/mm = 0.6 and 0.9 by using $w_{0.3}(z)$ in eq 1 as an adjustable parameter. Here $I(\mu;z)$ is an interpolated μ dependence of (100) diffraction at a given z between z/mm = 0.3 and 1.2, $I_{0.3}(\mu)$ and $I_{1.2}(\mu)$ are the μ dependence of (100) diffraction intensity in the measured 2D SAXS patterns at z/mm = 0.3 and 1.2, respectively, and $w_{0.3}(z)$ is the weighted contribution of $I_{0.3}(\mu)$ to $I(\mu;z)$. The best fit between the measured and calculated $I(\mu;z)$ yielded $w_{0.3}$ = 1.0, 0.8, 0.4, and 0.0 at z/mm = 0.3, 0.6, 0.9, and 1.2, respectively, as will be given below.

$I(\mu;z)$ calculated at z/mm = 0.6 and 0.9 (solid lines) are compared with the corresponding measured data (open circle) in parts b and c of Figure 4, respectively. In Figure 4b, the measured profile at z/mm = 0.6 fits well with the calculated profile obtained with $w_{0.3}(z/\text{mm} = 0.6) = 0.8$, so that the glass-surface-induced ordering is dominant at z/mm = 0.6. On the other hand, the measured profile at z/mm = 0.9 shown in Figure 4c fits well with the calculated profile obtained with $w_{0.3}(z/\text{mm} = 0.9) = 0.4$, implyng that the ∇T-induced ordering is dominant at z/mm = 0.9.

Moreover, the 2D SAXS patterns at z/mm = 0.6 and 0.9 also were calculated by using two-dimensional pattern at z/mm = 0.3 and 1.2 together with eq 1 and estimated values $w_{0.3}(z/\text{mm} = 0.6) = 0.8$ and $w_{0.3}(z/\text{mm} = 0.9) = 0.4$, respectively. The calculated patterns (shown in Figure 3e,f) are compared with the measured patterns shown in Figure 3b,c, respectively. The calculated patterns satisfactorily fit with the corresponding measured patterns. The weight $w_{0.3}$ decrease gradually with z, indicating that the crossover from the glass-surface-induced ordering to the moving-∇T-induced ordering occurs continuously.

4.3. A Possible Model for Crossover from Glass-Surface-Induced Ordering to ∇T-Induced Ordering. We would like to present here a possible model to explain the crossover process and mechanism from the glass-surface-induced ordering to the ∇T-induced ordering. We would like to leave checks on the validity of the model with experiments other than SAXS as future works.

The crossover may be explained by considering anisotropy in the growth rate of the grain of hex-cyl.[16,17] As shown in Figure 6a, it is found that the growth rate of the grain along the direction perpendicular to the cylinder axis (v_{90}) is larger than that parallel to the cylinder axis (v_0), giving rise to grains having an oblate ellipsoidal shape with the symmetry axis parallel to the cylinder axis. This anisotropy may bring about the crossover describe-dabove, through the processes from b-1 to b-4 shown in Figure 6b. In Figure 6b-1, the grain A shows the one developed through the glass-surface-induced ordering where the straight lines schematically indicate the (100) planes of hex-cyl shown in Figure 5a. The surface of the grain A grown from the glass surface will be exposed to the region α which is undercooled disordered state at $T < T_{ODT}$, when the growth rate of the grain A along ∇T direction ($v' = v_{90}\cos 45°$) is smaller than R. The other region of the specimen (the region on the right-hand side of the region α) is above T_{ODT} and hence is in the disordered state.

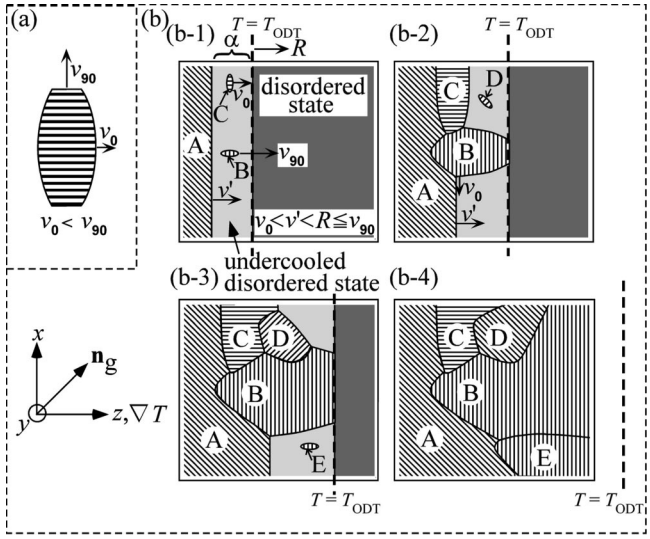

Figure 6. (a) Schematic illustration for anisotropic growth of the hex-cyl grain: the growth rate of the grain perpendicular to the cylinder axis v_{90} is larger than that parallel to the cylinder axis v_0. (b) Schematic illustration indicating the transition from the glass-surface-induced ordering (b-1) to the moving-∇T-induced ordering (b-4) on the basis of the anisotropic growth of hex-cyl grains. The grains B and E which have a largest growth rate along the ∇T direction become dominant with increase of z and hence with increase of time.

In this case in the region α, nucleation and growth of the grains having a random orientation of grains may occur as schematically and representatively shown by the grains B and C, resulting in the evolution of the randomly distributed orientation of hex-cyl. This scenario may provide a plausible explanation for the SAXS pattern observed at z/mm = 0.3 (Figure 3a). During the front plane of $T = T_{ODT}$ (shown by the dashed lines in parts b-1 to b-4) in the ∇T zone moves to the right-hand side, the grains A, B, and C grow as shown in Figure 6b-2. The growth rate of the grains A, B, and C along the ∇T direction are v', v_{90}, and v_0 ($v_0 < v' < R \leq v_{90}$), respectively, so that only the grain B can follow the displacement of the front plane of $T = T_{ODT}$ at the rate R. Here, the fact that $R \leq v_{90}$ is necessary to obtain the specific texture and orientation of hex-cyl inherent in the zone-heated specimens was found in our previous paper:[1] In fact, the moving rate $R = 75$ nm/s was found to satisfy the condition $R \leq v_{90}$. While the grain B continues to grow and follow the displacement of the front plane at the rate R, it can also grow laterally along the x axis and the y axis at the growth rate of v_0 and become dominant over other grains such as A, C, and D (as schematically illustrated in Figure 6b-3,b-4). On the other hand, the growth of the grain C along ∇T direction will be interrupted by the nucleation and growth of D and by the growth of the grain B. The growth of the grainA along the ∇T direction will be also interrupted by that of the grain B, C, and E. Thus, only the grain whose growth rate along the ∇T direction is the largest should become dominant over other grains.

In the moving-∇T-induced ordering shown in Figure 5b, not only the cylinder axis is perpendicular to the ∇T direction but also (100) plane of hex-cyl is perpendicular to the ∇T direction. This selection of lattice plane can be explained by the scenario as described above.

The selection can be explained by the following alternative scenario also, based upon stability of various Fourier modes of the concentration fluctuations in the disordered state. While the all Fourier modes of the concentration fluctuations in the region of disordered melts far away from the T_{ODT} front plane (e.g., the Fourier modes with wave vectors $\mathbf{q}_\perp$ and $\mathbf{q}_\parallel$ in region II in Figure 7a) have the same thermal stability, the stability of the Fourier modes very close to T_{ODT} (region I) depends on orientation of their wave vectors $\mathbf{q}$. The Fourier modes having their wave vectors parallel to the ∇T axis ($\mathbf{q}_\parallel$ in region I in Figure 7a) becomes more unstable than those having their wave vectors directing toward directions other than the ∇T axis (e.g., the wave vectors perpendicular to the ∇T axis, $\mathbf{q}_\perp$ in region I in Figure 7a). This is because the thermal correlation length ($\xi_\parallel$ or $\xi_\perp$) of these Fourier modes near T_{ODT} becomes very large so that the Fourier modes having wave vector $\mathbf{q}_\parallel$ extend into the region of undercooled disordered melts, while those having $\mathbf{q}_\perp$ do not. This makes the modes $\mathbf{q}_\parallel$ be selected for ordering. Hence, these selected Fourier modes, i.e., the plane wave fluctuations with wave vectors parallel to the ∇T axis as shown in Figure 7b-1, tend to order into the lamellar structure. However, the ordering into lamellae will not be actually allowed because of asymmetry of molecular volume of the constituent bcp chains. Hence, the plane wave fluctuations tend to be transformed into hex-cyl upon ordering, keeping their cylinder axes in the plane normal to the ∇T axis and randomly oriented around the ∇T axis, as schematically shown in Figure 7b-2. This ordering process is similar to the order−order transition from lamellae to hex-cyl,[18,19] and the "plane" of the plane wave fluctuations transform into (100) plane of hex-cyl as shown in Figure 7b-2,b-3. Thus, the moving ∇T also can induce the directed ordering into the columnar grains having the characteristic orientation of hex-cyl, initiated from the interface between the undercooled disordered phase and disordered phase. The columnar grains grown from this interface (designated hereafter "interface-induced ordering") are expected to be essentially the same as those grown from the glass surface (see Figure 14 in ref 1) for the case of $\mathbf{n}_g$ parallel to ∇T axis.

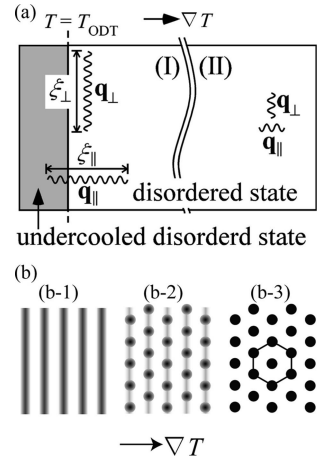

Figure 7. (a) Schematic illustration indicating the difference in thermal stability of Fourier modes of concentration fluctuations in the disordered state. In the region of disordered melts very close to T_{ODT} (region I), the Fourier modes having their wave vector parallel to the ∇T axis ($\mathbf{q}_\parallel$) becomes more unstable than those having their wave vectors in the directions other than the ∇T axis [e.g., wave vectors perpendicular to the ∇T axis ($\mathbf{q}_\perp$)]. In the region of disordered melts far away from T_{ODT} (region II), all Fourier modes of fluctuations have the same stability. (b) In the region of the disordered state very close to the T_{ODT} front, the plane wave fluctuations with the wave vector $\mathbf{q}_\parallel$ (b-1) is selected to order in the undercooled disordered state and transformed into ordered state (b-2 and b-3). The "plane" of the plane wave fluctuations is transformed into the (100) plane of hex-cyl.

4.4. Comparison with Previous Work. The results obtained in this work on the crossover behavior from the glass-surface-induced ordering to the moving ∇T-field-induced ordering of the hex-cyl forming bcp are found to be consistent with those reported by Hashimoto et al.[8] on the lamellar forming bcp. Those two experiments were conducted about the same ∇T, with the specimens having about equal T_{ODT}, and with slow enough but slightly different moving rates ($R = 75$ nm/s in this work and 400 nm/s in the previous work[8]).

Both cases commonly showed a crossover from dominance of the glass-surface-induced ordering near the glass surface to

Table 2. Comparison of Our Experiments and the Experiments by Berry et al.[12]

	bcps	zone-heating condition: type	R (μm/s)	thickness	∇T (°C/mm)	ξ	orientation[a]
Berry et al.	PS-*b*-PMMA	CZA	1−500	168 nm	17	100−2000 nm	parallel
our work	PS-*b*-PI	HZA	0.075	2 mm	42	∼mm	perpendicular

[a] Orientation of cylinder axis with respect to the ∇T axis is defined parallel and perpendicular when the cylinder axis is parallel and perpendicular to the moving ∇T axis (i.e., z axis), respectively.

dominance of the ∇T-field-induced ordering away from the glass surface at the same distance of $z \approx 1$ mm. We note the following points also commonly for the two cases: The glass-surface-induced ordering orients the lamellar normal $\mathbf{n}_l$ or the reciprocal lattice vector of (100) plane for hex-cyl $\mathbf{n}_{(100)}$ parallel to $\mathbf{n}_g$, while the ∇T-field-induced ordering orients $\mathbf{n}_l$ or $\mathbf{n}_{(100)}$ parallel to ∇T axis. The ∇T-field-induced ordering gives the six-point pattern for hex-cyl, while it gives two-arc or two-point pattern for lamellae, which is a difference inherent in the two systems (two-dimensional order vs one-dimensional order). In this work we quantitatively elucidated the crossover behavior and presented a possible mechanism and process of the crossover behavior, both of which were not dealt with in the previous paper.[8]

The moving-∇T field effects were also studied computationally[10,11] and experimentally[12,13] for two-dimensional (2D) systems and for thin bcp films, respectively. Zhang et al.[10] conducted 2D computational studies of the zone heating on symmetric ($f = 0.5$) and asymmetric ($f = 0.4$) bcps from the disordered state, where f is the volume fraction of the one block in dibcp. Bosse et al.[11] studied 2D simulation of the "cold zone annealing" (CZA) on the lamellar forming dibcp. In CZA, the zone heating is imposed on the initially disordered bcp under the condition where the highest temperature T_H satisfies $T_g < T_H < T_{ODT}$. In contrast to the CZA, the zone heating employed in this work and in the work by Zhan et al. can be designated as " hot zone annealing" (HZA) because $T_H > T_{ODT}$. Berry et al.[12] conducted the CZA for hex-cyl forming polystyrene-*block*-poly(methyl methacrylate) (PS-*b*-PMMA) spun-cast thin films of thickness about 6.5 times the Bragg spacing of hex-cyl.

First of all, it is difficult to compare our results on HZA of bulk bcps with those on HZA or CZA of the 2D systems and/or the thin films. Despite of the difference in the system's dimensionality (3D vs 2D), there is one important difference between our systems and the other systems. In our case the ordering under the HZA is affected by the surface or interface, either the glass surface or the interface between the well-ordered microdomain region and the supercooled disordered region or the interface between the supercooled disordered region and disordered region above T_{ODT}. This surface or interface exists normal to the ∇T axis (z axis) and causes sequential ordering of lamellae or hex-cyl with $\mathbf{n}_l$ or $\mathbf{n}_{(100)}$ parallel to the ∇T axis, respectively, as the ∇T front moves along the z axis.This kind of surface or interface does not seem to exist in other systems.[10–12] The 2D simulations[10,11] showed that the lamellar orientation varies with decreasing the moving rate R from the "parallel orientation" with their interfaces parallel to the ∇Tfront to the "perpendicular orientation" with their interfaces normal to the front. The former orientation is apparently consistent with our case.

Table 2 summarizes comparisons between our experiments and the experiments by Berry et al.[12] The type of the zone heating (CZA and HZA), moving rate R, and sample thickness are obviously quite different. The CZA experiments on the thin PS-*b*-PMMA at a low moving rate R ($= 1$ μm/s) by Berry et al. showed the cylinder axis orients preferentially along the ∇T axis, which is opposite to our results. The difference is not well understood at this moment. The correlation length ξ for the orientation of hex-cyl attained in the zone-heated specimens was also very different (mesoscopic vs macroscopic). Berry et al. attained $\xi = 100-2000$ nm, while we attained $\xi \approx 2$ mm (see the z-dependence of the SAXS pattern shown in Figures 7 and 9 in ref 1).

5. Concluding Remarks

We elucidated that the zone-heating method with the tilted glass surface imposed on the bulk cylinder forming bcp can separate the glass-surface-induced ordering from the ∇T-field-induced ordering. The glass-surface-induced ordering dominates near the glass surface, while the ∇T-field-induced ordering dominates away from the glass surface; under the given zone-heating condition, the crossover occurs at $z \approx 1$ mm. Thus, we could prove that the ∇T field itself creates the macroscopically extended columnar grain of hex-cyl, independently from the glass-surface-induced ordering. The crossover from the glass-surface-induced ordering to the ∇T-field-induced ordering with increasing distance z from the glass surface was quantitatively clarified for the first time in this paper by the positional dependence of the SAXS patterns (section 4.2). A possible model to explain the crossover was also presented in section 4.3.

References and Notes

(1) Mita, K.; Tanaka, H.; Saijo, K.; Takenaka, M.; Hashimoto, T. *Macromolecules* **2007**, *40*, 5923.
(2) Fredrickson, G. H. *Macromolecules* **1987**, *20*, 2535.
(3) Fredrickson, G. H.; Helfand, E. *J. Chem. Phys.* **1988**, *89*, 5890.
(4) Menelle, A.; Russel, T. P.; Anastasiadis, S. H.; Satija, S. K.; Majkrzak, C. F. *Phys. Rev. Lett.* **1992**, *68*, 67.
(5) Lambooy, P.; Russel, T. P.; Kellogg, G. J.; Mayes, A. M.; Gallagher, P. D.; Satija, S. K. *Phys. Rev. Lett.* **1994**, *72*, 2899.
(6) Koneripalli, N.; Singh, N.; Levicky, R.; Bates, F. S.; Gallagher, P. D.; Satija, S. K. *Macromolecules* **1995**, *28*, 2897.
(7) Binder, K. *Acta Polym.* **1995**, *46*, 204.
(8) Hashimoto, T.; Bodycomb, J.; Funaki, Y.; Kimishima, K. *Macromolecules* **1999**, *32*, 952.
(9) Bodycomb, J.; Funaki, Y.; Kimishima, K.; Hashimoto, T. *Macromolecules* **1999**, *32*, 2075.
(10) Zhang, H.; Zhang, J.; Yang, Y.; Zhou, X. *J. Chem. Phys.* **1997**, *106*, 784.
(11) Bosse, A. W.; Douglass, J. F.; Berry, B. C.; Jones, R. L.; Karim, A. *Phys. Rev. Lett.* **2007**, *99*, 216101.
(12) Berry, B. C.; Bosse, A. W.; Douglass, J. F.; Jones, R. L.; Karim, A. *Nano Lett.* **2007**, *7*, 2789.
(13) Angelescu, D. E.; Waller, J. H.; Adamson, D. H.; Register, R. A.; Chaikin, P. M. *Adv. Mater.* **2007**, *19*, 2687.
(14) In ref 1 we described that we used the poly(ethylene terephthalate) (PET) sheets in order to confine 2 mm thick film. This is a mistake. Actually, we used polyimide sheets called Kapton.
(15) Hashimoto, T.; Okamoto, S.; Saijo, K.; Kimishima, K.; Kume, T. *Acta Polym.* **1995**, *46*, 463.
(16) Koizumi, S.; Hasegawa, H.; Hashimoto, T. *Macromolecules* **1994**, *27*, 6532.
(17) Sakamoto, N.; Hashimoto, T. *Macromolecules* **1998**, *31*, 8493.
(18) Sakurai, S.; Momii, T.; Taie, K.; Shibayama, M.; Nomura, S.; Hashimoto, T. *Macromolecules* **1993**, *26*, 485.
(19) Hajduk, D. A.; Gruner, S. M.; Rangarajan, P.; Register, R. A.; Fetters, L. J.; Honeker, C.; Albalak, R. J.; Thomas, E. L. *Macromolecules* **1994**, *27*, 490.
(20) Schrader, D. In *Polymer Handbook*, 4th ed.; Brandrup, J., Immergut, E. H., Grulke, E. A., Eds.; John Wiley & Sons: New York, 1999; p V-91.
(21) Furuta, I. Kimura, S. Iwama, M. In *Polymer Handbook*, 4th ed.; Brandrup, J., Immergut, E. H., Grulke, E. A., Eds.; John Wiley & Sons: New York, 1999; p V-5.

MA800361D